Enhancing Coherent Light-Matter Interactions through Microcavity-Engineered Plasmonic Resonances

Pai Peng (彭湃),[1,*] Yong-Chun Liu,[2] Da Xu,[1] Qi-Tao Cao,[1] Guowei Lu,[1,3] Qihuang Gong,[1,3] and Yun-Feng Xiao[1,3,†]

[1]*State Key Laboratory for Mesoscopic Physics and School of Physics, Peking University; Collaborative Innovation Center of Quantum Matter, Beijing 100871, People's Republic of China*

[2]*State Key Laboratory of Low-Dimensional Quantum Physics and Department of Physics, Tsinghua Univeristy, Beijing 100084, People's Republic of China*

[3]*Collaborative Innovation Center of Extreme Optics, Shanxi University, Taiyuan, 030006 Shanxi, People's Republic of China*

(Received 23 May 2017; published 4 December 2017; corrected 28 December 2017)

Quantum manipulation is challenging in localized-surface plasmon resonances (LSPRs) due to strong dissipations. To enhance quantum coherence, here we propose to engineer the electromagnetic environment of LSPRs by placing metallic nanoparticles (MNPs) in optical microcavities. An analytical quantum model is first built to describe the LSPR-microcavity interaction, revealing the significantly enhanced coherent radiation and the reduced incoherent dissipation. Furthermore, when a quantum emitter interacts with the LSPRs in the cavity-engineered environment, its quantum yield is enhanced over 40 times and the radiative power over one order of magnitude, compared to those in the vacuum environment. Importantly, the cavity-engineered MNP-emitter system can enter the strong coupling regime of cavity quantum electrodynamics, providing a promising platform for the study of quantum plasmonics, quantum information processing, precise sensing, and spectroscopy.

DOI: 10.1103/PhysRevLett.119.233901

Coherent light-matter interactions lay the foundation for studies in quantum optics and applications ranging from quantum sensing to quantum information processing [1]. So far, various optical systems have been developed to tailor the coupling between quantum emitters and photons [2–4]. An emerging field is the study of light-matter interactions at the nanoscale between few or even single quantum emitters and localized-surface plasmon resonances (LSPRs) in metallic nanostructures [4]. For example, in the weak coupling regime where the incoherent dissipation dominates, LSPRs are widely used to enhance fluorescence [5–7] and Raman scattering [8–10] and to achieve unidirectional emission [11]; in the strong coupling regime where the coherent interaction dominates, hybridizations between plasmonic resonances and quantum emitters have also been investigated both theoretically [12–17] and experimentally [18–25].

Two approaches have been taken to achieve single-emitter strong coupling—reducing the mode volumes and suppressing the dissipations. The former typically requires ultrafine geometries with nanometer or even subnanometer precision [19,24], posing challenges on fabricating metallic structures and positioning individual quantum emitters. For the latter, the dipolar plasmonic modes dissipate through both radiation and Ohmic absorption, while the multipole modes are purely absorptive [26]. Better coherence can be achieved by reducing the excitation of multipole modes or enhancing the excitation of dipolar modes. Thus, efforts have been made to tailor the geometry of the metallic nanostructures, for example, elongating metallic nanoparticles (MNPs) to separate the dipolar and multipole resonances [27], and forming dimers or arrays to obtain stronger coupling of a certain dipolar mode [28]. An alternative approach is canceling the coupling between the emitters and the multipole modes with the emitters homogeneously distributed around the metallic structure [29]. Despite these efforts, the nonradiative decay from the dipolar plasmonic modes remains serious for small metallic nanostructures which are advantageous for stronger light-matter interactions brought by more confined fields [10]. Hybrid plasmonic-photonic modes have been reported in various systems [30–46] where LSPRs magnify the cavity field, creating local hot spots [37–40] and enhancing sensing sensitivity [41–46]. The treatment of hybrid modes, however, typically oversimplifies the dynamical response of LSPRs and obscures the role of each component. Here, by building a full quantum model, we reveal that the microcavity engineers the electromagnetic environment of the dipolar plasmonic mode, enhancing its radiation rate and further reducing the Ohmic absorption. When a single quantum emitter interacts with the cavity-engineered LSPRs, the quantum yield is boosted more than 40-fold, and the radiative power is enhanced over one order of magnitude, compared to LSPRs in vacuum. With the better coherence, vacuum Rabi oscillation, vacuum Rabi splitting, and anticrossing phenomena arise, manifesting the cavity-engineered MNP-emitter system in the strong coupling regime.

We develop an analytical model to describe the cavity-engineered LSPRs interacting with a quantum emitter,

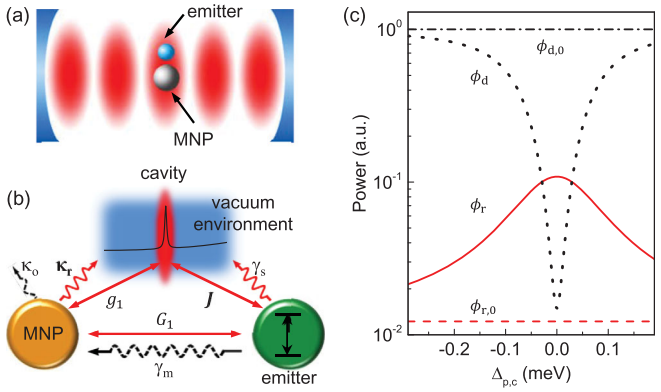

FIG. 1. (a) A quantum emitter coupled to a MNP in a microcavity-engineered electromagnetic environment. (b) Schematic of the interaction in the system. The cavity results in a peak in vacuum density of state, marked by the red region. (c) Power outputs in logarithmic scale of the LSPR to each channel versus the pump-cavity detuning $\Delta_{p,c} = \omega_p - \omega_c$: radiation with cavity ϕ_r (red solid curve), radiation without cavity $\phi_{r,0}$ (red dashed curve), absorption with cavity ϕ_d (black dots), and absorption without cavity $\phi_{d,0}$ (black dash-dotted curve).

shown in Fig. 1(a). The quantum emitter is assembled onto the MNP surface, and the composite is placed inside an optical microcavity. The electromagnetic environment of LSPRs is thus formed by both the cavity mode and vacuum. First we study how the microcavity engineers the electromagnetic environment of LSPRs in the absence of the quantum emitter. The Hamiltonian contains three parts: $H = H_c + H_m + H_I$. Here $H_c = \omega_c \hat{c}^\dagger \hat{c}$ characterizes the cavity mode $\hat{c}$ with resonance frequency ω_c. To simplify the discussion without loss of generality, we focus on spherical particles if not mentioned, so $H_m = \sum_l \omega_l \hat{a}_l^\dagger \hat{a}_l$ describing the quantized plasmonic modes $\hat{a}_l$ with resonance frequencies ω_l [4,47], where $l = 1, 2, \ldots$ labels the mode order (dipole, quadrupole, etc). Furthermore, we consider particles with scale much smaller than wavelength to apply quasistatic approximation, so that only dipolar LSPR ($l = 1$) is coupled to the cavity field [48]. The interaction Hamiltonian then reads $H_I = g_1(\hat{a}_1^\dagger + \hat{a}_1)(\hat{c}^\dagger + \hat{c})$, with g_1 being the coupling coefficient between the cavity and the dipolar plasmonic mode, shown in Fig. 1(b). Validity of the quantization is discussed in detail in Ref. [48]. Thus, the quantum Langevin equations are given as [49]

$$\frac{d\hat{c}}{dt} = -\left(i\omega_c + \frac{\kappa_c}{2}\right)\hat{c} - ig_1\hat{a}_1 + \hat{F}_c, \tag{1a}$$

$$\frac{d\hat{a}_1}{dt} = -\left(i\omega_1 + \frac{\kappa_1}{2}\right)\hat{a}_1 - ig_1\hat{c} - \sqrt{\kappa_{\rm in}}\hat{a}_{\rm in} + \hat{F}_1, \tag{1b}$$

where $\hbar$ is set to be 1, κ_c, and κ_1 are the decay rates of the cavity and the dipolar plasmonic modes; the input operator $\hat{a}_{\rm in}$ represents the optical pump to the dipolar plasmonic mode, at rate $\kappa_{\rm in}$ and frequency ω_p; $\hat{F}_c$ and $\hat{F}_1$ are the noise operators, with $\langle \hat{F}_c^\dagger(t)\hat{F}_c(t')\rangle \approx 0$ and $\langle \hat{F}_1^\dagger(t)\hat{F}_1(t')\rangle \approx 0$ at optical frequencies.

The resonance frequency of the dipolar plasmonic mode $\omega_1 = 2.3$ eV is determined using the Drude model [48]. The dipolar mode has two dissipation channels: radiation of rate κ_r and Ohmic loss of rate κ_o, with the total decay rate $\kappa_1 = \kappa_r + \kappa_o$. We consider a gold nanoparticle with $\kappa_o = 0.2$ eV extracted from Ref. [50]. The radiative decay rate is $\kappa_r = 2.45$ meV, calculated following Ref. [47]. By setting the cavity mode volume to be 1 μm^3 and the quality factor $Q = 10^5$, we compare the analytical results with the numerical results computed from Mie theory and find good agreement for the MNP radius $R < 30$ nm [48]. Therefore, we set radius $R = 10$ nm if not stated. The coupling coefficient between the dipolar plasmonic mode and the cavity mode is $g_1 = -2.9$ meV [48].

In the following, we study the steady-state solution of Eq. (1). To characterize the dissipative property of microcavity-engineered plasmonic excitation, we calculate the dissipation power using the input-output formulation [49]. The radiative output power (in the unit of photon energy $\hbar\omega_p$, the same below) $\phi_r = \kappa_r\langle \hat{a}_1^\dagger \hat{a}_1\rangle + \kappa_c\langle \hat{c}^\dagger \hat{c}\rangle$ is comprised of (i) radiation from the MNP to vacuum and (ii) coupling into the cavity for further guiding. The Ohmic dissipation power of the dipolar plasmonic mode is given by $\phi_d = \kappa_o\langle \hat{a}_1^\dagger \hat{a}_1\rangle$. When the cavity and the dipolar plasmonic mode are on resonance ($\omega_1 = \omega_c$), the radiation power and the absorption power of the cavity-engineered plasmonic mode are compared to the bare plasmon case in Fig. 1(c) [48]. It is shown that Ohmic loss dominates over radiation in the absence of the microcavity. While in the presence of the cavity, the radiation is enhanced by over one order of magnitude, and Ohmic absorption is reduced by almost 2 orders of magnitude on cavity resonance. This phenomenon is attributed to the nontrivial electromagnetic environment created by the cavity, giving rise to an enhanced radiation of dipolar LSPR. The radiation to the cavity environment then guides the energy out from the absorptive region, resulting in the reduction of incoherent absorption.

With the property of enhanced coherence, we show that the cavity-engineered LSPRs exhibit unique advantages in the coherent manipulation of a quantum emitter. After introducing an emitter, the quantum Langevin equation is given by [48]

$$\frac{d\hat{c}}{dt} = -\left(i\omega_c + \frac{\kappa_c}{2}\right)\hat{c} - ig_1\hat{a}_1 - iJ\hat{\sigma}_- + \hat{F}_c, \tag{2a}$$

$$\frac{d\hat{a}_1}{dt} = -\left(i\omega_1 + \frac{\kappa_1}{2}\right)\hat{a}_1 - ig_1\hat{c} - iG_1\hat{\sigma}_- + \hat{F}_1, \tag{2b}$$

$$\frac{d\hat{\sigma}_-}{dt} = -\left(i\omega_e + \frac{\gamma_e}{2}\right)\hat{\sigma}_- + i\hat{\sigma}_z(J\hat{c} + G_1\hat{a}_1) - \sqrt{\gamma_{\rm in}}\hat{\sigma}_{{\rm in},-} + \hat{F}_e, \tag{2c}$$

where $\hat{\sigma}_- = |g\rangle\langle e| = \hat{\sigma}_+^\dagger$ denotes the lowering operator of the emitter, with $|g\rangle$ ($|e\rangle$) being the ground (excited) state; $\hat{\sigma}_z = |e\rangle\langle e| - |g\rangle\langle g|$; ω_e is the transition frequency of the emitter; G_1 (J) indicates the coupling coefficient between the emitter and the dipolar plasmonic mode (cavity); the input operator $\hat{\sigma}_{\text{in},-}$ represents the optical pump to the emitter, at rate γ_{in} and frequency ω_p; $\hat{F}_e$ is the noise operator satisfying $\langle \hat{F}_e^\dagger(t)\hat{F}_e(t')\rangle \approx 0$ at optical frequencies. The multipole plasmonic modes can be characterized by a Markovian heat bath interacting with the quantum emitter [48]. As a result, the decay rate of the emitter is $\gamma_e = \gamma_s + \gamma_m$, consisting of the radiation to vacuum with rate γ_s and the dissipation to multipole plasmonic modes with rate γ_m [48].

We calculate the quantum yield and radiative power of the emitter in the weak pumping limit; i.e., the emitter is predominantly in the ground state, so that the operator $\hat{\sigma}_z$ in Eq. (2) can be replaced by its expectation value $\langle \sigma_z \rangle \approx -1$. The quantum yield is defined as $\eta = \Phi_r/(\Phi_r + \Phi_d)$ [5]. The radiative output power $\Phi_r = \langle(\sqrt{\kappa_r}\hat{a}_1^\dagger + \sqrt{\gamma_s}\hat{\sigma}_+)(\sqrt{\kappa_r}\hat{a}_1 + \sqrt{\gamma_s}\hat{\sigma}_-)\rangle + \kappa_c\langle\hat{c}^\dagger\hat{c}\rangle$, where the first term represents the radiation to vacuum from both the emitter and the dipolar plamonic mode, and the second term denotes the output through the cavity. The Ohmic dissipation power $\Phi_d = \kappa_o\langle\hat{a}_1^\dagger\hat{a}_1\rangle + \gamma_m\langle\hat{\sigma}_+\hat{\sigma}_-\rangle$, contributed from the both dipolar (first term) and multipole plasmonic mode (second term). In Fig. 2(a) we plot the steady-state

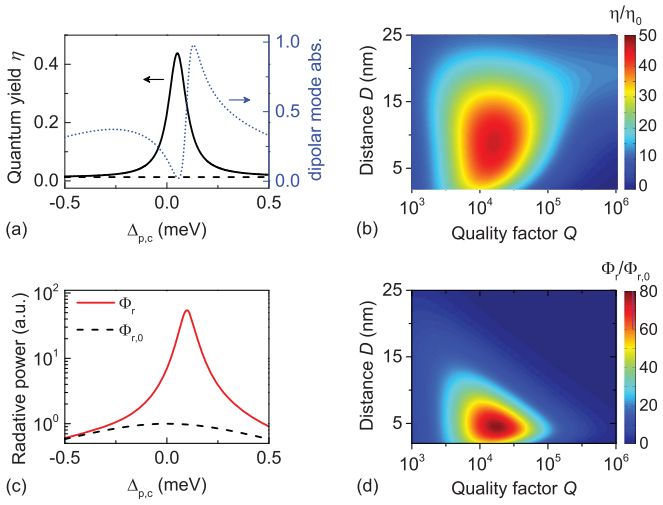

FIG. 2. (a) Quantum yield (left axis) and normalized dipolar mode absorption (right axis) versus the pump-cavity detuning $\Delta_{p,c}$. The black solid curve (dashed line) plots quantum yield η (η_0) with (without) the cavity. (b) Enhancement factor of quantum yield η/η_0 versus the distance D and the cavity Q factor. (c) Radiative power spectrum with the cavity Φ_r (red solid curve) and without the cavity $\Phi_{r,0}$ (black dashed curve). (d) Enhancement factor of radiative power $\Phi_r/\Phi_{r,0}$ versus the distance D and the cavity Q factor. In (a) to (d), the parameters are $\{J, G, \gamma_s, \gamma_m\} = \{-144, -7200, 3, 83\}$ μeV; the cavity, emitter, and dipolar LSPR are on resonance, i.e., $\omega_c = \omega_e = \omega_1$. In (b) and (d), $\Delta_{p,c} = \Delta_0$.

results of quantum yield η for an emitter with dipole moment $\mu = 1\ e \cdot \text{nm}$ and the distance $D = 10$ nm between the emitter and the MNP surface. It shows that the quantum yield $\eta > 40\%$ in the presence of the cavity, while the quantum yield is $\eta_0 = 1\%$ for the bare MNP case. This significant enhancement of quantum yield results from microcavity-reduced plasmonic absorption, demonstrated by the blue dotted curve in Fig. 2(a). The maximum quantum yield corresponds to the valley in the Fano line-shape absorption spectrum of the dipolar mode. Note that the Fano resonance originates from the interference of two channels that excite the dipolar modes—(i) direct excitation from the quantum emitter and (ii) indirect excitation from the emitter through cavity to dipolar mode, see Fig. 1(b). Maximum destructive interference is achieved when the pump-cavity detuning $\Delta_{p,c}$ satisfies [48]

$$\Delta_{p,c} = -J\frac{g_1}{G_1} \equiv \Delta_0. \tag{3}$$

The peak of the LSPR excitation does not correspond to the minimum of quantum yield because both the Ohmic loss and the radiation power are strong. Although the excitation of LSPR is reduced at $\Delta_{p,c} = \Delta_0$, compromising the local density of state near the quantum emitter, radiation enhancement due to the cavity environment still leads to over one-order-of-magnitude larger output power Φ_r in comparison with the bare MNP case $\Phi_{r,0}$, as shown in Fig. 2(c).

Figures 2(b) and 2(d) plot, respectively, the enhancement factors of the quantum yield η/η_0 and the radiative power $\Phi_r/\Phi_{r,0}$ versus the emitter-MNP distance D and the cavity Q factor. It is counterintuitive that the engineering effect of the microcavity does not increase monotonically with increasing Q, instead it has a maximum at Q^{opt}. This phenomenon is attributed to two counteracting effects: (i) when $Q < Q^{\text{opt}}$, absorption of dipolar plasmonic mode dominates the energy dissipation, because the electromagnetic environment of a broad cavity resonance is basically the same as vacuum; (ii) when $Q > Q^{\text{opt}}$, although the dipolar plasmonic mode dissipates most of its energy through radiation, the energy guiding channel through the cavity becomes less efficient for a high Q factor, so that a substantial portion of energy is absorbed by multipole modes. Balance of the two effects leads to a maximum radiation enhancement at $Q = Q^{\text{opt}}$. Figures 2(b) and 2(d) show that the effect of cavity engineering also depends on the emitter-MNP distance D. When D is small, the loss from the multipole plasmonic modes dominates; for a large D, the coupling between the emitter and LSPRs becomes weaker. In the present case, the over 20-fold radiation enhancement can be achieved in a wide range, $5\ \text{nm} < D < 15\ \text{nm}$.

The reduction of the incoherent absorption is able to bring the originally weak-coupled emitter-MNP system into the strong coupling regime. Different from the previous semiclassical treatment of the hybrid photonic-plasmonic mode

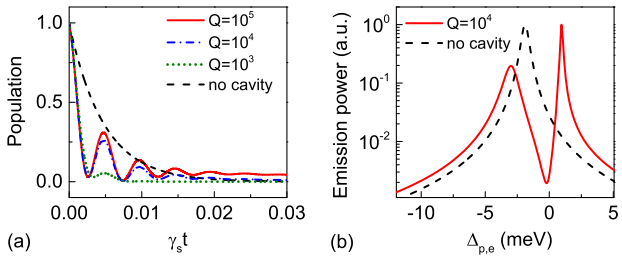

FIG. 3. (a) Temporal evolution of the population $\langle\hat{\sigma}_+(t)\hat{\sigma}_-(t)\rangle$ on the emitter for $Q = 10^5$ (red solid curve), $Q = 10^4$ (blue dash-dotted curve), $Q = 10^3$ (green dots), and without the cavity (black dashed curve). (b) Radiation power of the emitter with respect to the pump-emitter detuning $\Delta_{p,e} = \omega_p - \omega_e$ for $Q = 10^4$ (red solid curve) and without the cavity (black dashed curve). In (a) and (b), included angle $\theta = 60°$, the emitter-MNP distance $D = 5$ nm, cavity mode volume is 0.1 μm^3, plasmonic mode volume is 400 nm^3, detunings $\omega_1 - \omega_e = 0.6$ eV and $\omega_c - \omega_e = 1.5$ meV.

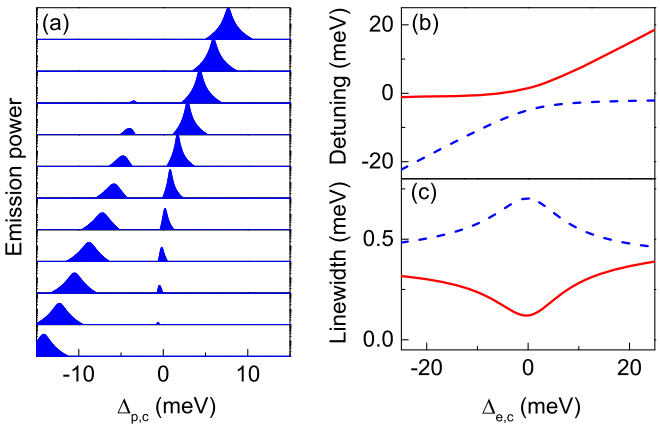

FIG. 4. (a) Emission spectra (in logarithmic scale) of the emitter for various $\Delta_{e,c}$. From bottom to top, $\Delta_{e,c}$ increases from −10 meV to 10 meV with a 2 meV step. (b) Detunings and (c) linewidths of the two eigenmodes formed in the strongly coupled cavity-engineered plasmonic mode and the emitter. Parameters are the same as in Fig. 3.

[37–39], we study the strong coupling dynamics using the full quantum model. To emphasize that the role of cavity is to engineer LSPRs, rather than to couple the emitter directly, we deliberately design the geometry of the system by setting the dipole moment of the emitter $\vec{\mu}$ perpendicular to cavity electric field $\vec{E}_{\rm cav}$, so that the cavity-emitter coupling $J = 0$. An ellipsoidal MNP with a large aspect ratio is used here, so that only the dipolar resonance along the long axis is considered [27]. By placing the long axis in the plane formed by $\vec{\mu}$ and $\vec{E}_{\rm cav}$, the dipolar plasmonic mode couples to both the cavity and the emitter, with coefficients $G_1(\theta) = G_1 \cos\theta$ and $g_1(\theta) = g_1 \sin\theta$, where θ is the included angle between the long axis and $\vec{E}_{\rm cav}$. The cavity-engineered MNP-emitter system exhibits the vacuum Rabi oscillation and splitting, the typical manifestations of strong coupling [Figs. 3(a) and 3(b)]. In the temporal domain, the emitter undergoes 5 complete periods of oscillation for $Q = 10^5$ [Fig. 3(a)]. As the quality factor decreases, the number of periods declines, and oscillation does not occur without the cavity, demonstrating that the cavity engineering is crucial for achieving strong coupling. In the frequency domain, the emission spectrum of the emitter $\gamma_s\langle\hat{\sigma}_+(\omega_p)\hat{\sigma}_-(\omega_p)\rangle$ exhibits two well-separated peaks for $Q = 10^4$ [Fig. 3(b)]. The emission spectra are further illustrated in Fig. 4(a) with different emitter-cavity detuning $\Delta_{e,c} = \omega_e - \omega_c$. The anticrossing shown in the spectra is studied by analyzing the eigenfrequencies and linewidths of the two involved eigenmodes [48,51], plotted in Figs. 4(b) and 4(c). The vacuum Rabi splitting $2g_{\rm eff}$ reaches 3.5 meV, larger than the linewidths of both eigenmodes $\Gamma_1 = 1.28$ meV and $\Gamma_2 = 0.11$ meV. The cooperativity $4g_{\rm eff}^2/(\Gamma_1\Gamma_2)$ exceeds 80. Dependence of cooperativity on relevant parameters is discussed in Ref. [48]. The linewidths do not show a crossed pattern as in the conventional cavity quantum electrodynamics (QED) case [49], because cavity mediated LSPR-emitter coupling poses both a dispersive and dissipative nature. The similar mechanism was reported in exciton mediated optomechanical coupling [52] and low-Q cavity mediated cavity QED coupling [53]. The dispersive coupling leads to the repulsion of the eigenfrequencies' real parts [Fig. 4(b)], and the dissipative coupling results in repulsion of the imaginary parts [Fig. 4(c)].

Finally we discuss the experimental feasibility. A single quantum emitter can be grafted onto a single MNP by using the DNA strands, with the controllable distance down to nanometer scale [54,55]. Further, the emitter-MNP composite can be bound to the microcavity by a second DNA strand via biotinylated bovine serum albumin [43,56]. The versatility of the DNA origami technique enables nanometer-scale precise construction of the cavity-MNP composite for a substantial overlap between the cavity field and LSPRs.

In summary, we propose to achieve the coherent light-matter interaction by engineering the electromagnetic environment of LSPRs using an optical microcavity. By constructing an analytic quantum model to describe the LSPRs-microcavity interaction, we find that the microcavity enhances the coherent radiation of the dipolar plasmonic mode, and thus reduces the incoherent Ohmic dissipation. When interacting with a quantum emitter, the microcavity-engineered LSPRs significantly enhance the quantum yield and the radiative power output, compared to those in the vacuum environment. Most importantly, with the dissipation suppressed, the microcavity-engineered MNP-emitter system can reach the strong coupling regime of cavity QED, while the bare MNP-emitter interaction falls into the weak coupling regime. In combination with previous approaches to suppressing the excitations of multipole modes [27–29], the engineered plasmonics promotes quantum optical applications such as fast single-photon generation, quantum logic gates, and entanglement [57–59].

We thank Xi Chen and Linbo Shao at Harvard University and Heming Wang at California Institute of Technology for fruitful discussions. This project was supported by the National Key R&D Program of China (Grant No. 2016YFA0301302) and the National Natural Science Foundation of China (Grants No. 61435001, No. 11654003, No. 11474011, No. 11527901, No. 11674390, and No. 91736106). P. P. was supported by the National Fund for Fostering Talents of Basic Science.

Note added.—Recently, we noted an independent work that studied a similar system using numerical simulation and the quasinormal mode approximation [60].

*Present address: Department of Electrical Engineering and Computer Science, Massachusetts Institute of Technology, Cambridge, Massachusetts 02139, USA.
†yfxiao@pku.edu.cn; www.phy.pku.edu.cn/~yfxiao/.

[1] H. J. Kimble, Nature (London) **453**, 1023 (2008).
[2] K. J. Vahala, Nature (London) **424**, 839 (2003).
[3] P. Lodahl, S. Mahmoodian, and S. Stobbe, Rev. Mod. Phys. **87**, 347 (2015).
[4] M. S. Tame, K. McEnery, Ş. Özdemir, J. Lee, S. Maier, and M. Kim, Nat. Phys. **9**, 329 (2013).
[5] S. Kühn, U. Håkanson, L. Rogobete, and V. Sandoghdar, Phys. Rev. Lett. **97**, 017402 (2006).
[6] L. Novotny and N. Van Hulst, Nat. Photonics **5**, 83 (2011).
[7] F. Tam, G. P. Goodrich, B. R. Johnson, and N. J. Halas, Nano Lett. **7**, 496 (2007).
[8] S. Nie and S. R. Emory, Science **275**, 1102 (1997).
[9] K. Kneipp, Y. Wang, H. Kneipp, L. T. Perelman, I. Itzkan, R. R. Dasari, and M. S. Feld, Phys. Rev. Lett. **78**, 1667 (1997).
[10] J. N. Anker, W. P. Hall, O. Lyandres, N. C. Shah, J. Zhao, and R. P. Van Duyne, Nat. Mater. **7**, 442 (2008).
[11] A. G. Curto, G. Volpe, T. H. Taminiau, M. P. Kreuzer, R. Quidant, and N. F. van Hulst, Science **329**, 930 (2010).
[12] A. Trügler and U. Hohenester, Phys. Rev. B **77**, 115403 (2008).
[13] A. Manjavacas, F. J. G. Abajo, and P. Nordlander, Nano Lett. **11**, 2318 (2011).
[14] T. Hümmer, F. J. García-Vidal, L. Martín-Moreno, and D. Zueco, Phys. Rev. B **87**, 115419 (2013).
[15] T. J. Antosiewicz, S. P. Apell, and T. Shegai, ACS Photonics **1**, 454 (2014).
[16] J. Yang, M. Perrin, and P. Lalanne, Phys. Rev. X **5**, 021008 (2015).
[17] J. Ren, Y. Gu, D. Zhao, F. Zhang, T. Zhang, and Q. Gong, Phys. Rev. Lett. **118**, 073604 (2017).
[18] D. E. Chang, A. S. Sørensen, E. A. Demler, E. A. Demler, and M. D. Lukin, Nat. Phys. **3**, 807 (2007).
[19] R. Chikkaraddy, B. de Nijs, F. Benz, S. J. Barrow, O. A. Scherman, E. Rosta, A. Demetriadou, P. Fox, O. Hess, and J. J. Baumberg, Nature (London) **535**, 127 (2016).
[20] K. Santhosh, O. Bitton, L. Chuntonov, and G. Haran, Nat. Commun. **7**, ncomms11823 (2016).
[21] J. Bellessa, C. Bonnand, J. C. Plenet, and J. Mugnier, Phys. Rev. Lett. **93**, 036404 (2004).
[22] G. Zengin, M. Wersäll, S. Nilsson, T. J. Antosiewicz, M. Käll, and T. Shegai, Phys. Rev. Lett. **114**, 157401 (2015).
[23] X. Cheng, Y.-H. Cheng, J. Qin, D. Zhao, B. Ding, R. J. Blaikie, and M. Qiu, Nano Lett. **17**, 3246 (2017).
[24] A. L. Rodarte and A. R. Tao, J. Phys. Chem. C **121**, 3496 (2017).
[25] R. Liu, Z.-K. Zhou, Y.-C. Yu, T. Zhang, H. Wang, G. Liu, Y. Wei, H. Chen, and X.-H. Wang, Phys. Rev. Lett. **118**, 237401 (2017).
[26] R. Ruppin, J. Chem. Phys. **76**, 1681 (1982).
[27] L. Rogobete, F. Kaminski, M. Agio, and V. Sandoghdar, Opt. Lett. **32**, 1623 (2007).
[28] O. L. Muskens, V. Giannini, J. A. Snchez-Gil, and J. G. Rivas, Nano Lett. **7**, 2871 (2007).
[29] A. Delga, J. Feist, J. Bravo-Abad, and F. J. Garcia-Vidal, Phys. Rev. Lett. **112**, 253601 (2014).
[30] N. D. Lanzillotti-Kimura, T. Zentgraf, and X. Zhang, Phys. Rev. B **86**, 045309 (2012).
[31] Y. Yin, S. Li, S. Böttner, F. Yuan, S. Giudicatti, E. Saei Ghareh Naz, L. Ma, and O. G. Schmidt, Phys. Rev. Lett. **116**, 253904 (2016).
[32] R. Ameling and H. Giessen, Nano Lett. **10**, 4394 (2010).
[33] A. Konrad, A. M. Kern, M. Brecht, and A. J. Meixner, Nano Lett. **15**, 4423 (2015).
[34] P. Wang, Y. Wang, Z. Yang, X. Guo, X. Lin, X.-C. Yu, Y.-F. Xiao, W. Fang, L. Zhang, G. Lu, Q. Gong, and L. Tong, Nano Lett. **15**, 7581 (2015).
[35] S. Liu, J. Li, R. Yu, and Y. Wu, Phys. Rev. A **87**, 042306 (2013).
[36] H. Takashima, K. Kitajima, Y. Tanaka, H. Fujiwara, and K. Sasaki, Phys. Rev. A **89**, 021801 (2014).
[37] Y.-F. Xiao, Y.-C. Liu, B.-B. Li, Y.-L. Chen, Y. Li, and Q. Gong, Phys. Rev. A **85**, 031805 (2012).
[38] N. P. de Leon, B. J. Shields, C. L. Yu, D. E. Englund, A. V. Akimov, M. D. Lukin, and H. Park, Phys. Rev. Lett. **108**, 226803 (2012).
[39] M. Frimmer and A. F. Koenderink, Phys. Rev. Lett. **110**, 217405 (2013).
[40] H. M. Doeleman, E. Verhagen, and A. F. Koenderink, ACS Photonics **3**, 1943 (2016).
[41] M. A. Santiago-Cordoba, S. V. Boriskina, F. Vollmer, and M. C. Demirel, Appl. Phys. Lett. **99**, 073701 (2011).
[42] S. I. Shopova, R. Rajmangal, R. Holler, and S. Arnold, Appl. Phys. Lett. **98**, 243104 (2011).
[43] J. D. Swaim, J. Knittel, and W. P. Bowen, Appl. Phys. Lett. **99**, 243109 (2011).
[44] Y.-F. Xiao, C.-L. Zou, B.-B. Li, Y. Li, C.-H. Dong, Z.-F. Han, and Q. Gong, Phys. Rev. Lett. **105**, 153902 (2010).
[45] M. A. Schmidt, D. Y. Lei, L. Wondraczek, V. Nazabal, and S. A. Maier, Nat. Commun. **3**, 1108 (2012).
[46] F. Gu, L. Zhang, Y. Zhu, and H. Zeng, Laser Photonics Rev. **9**, 682 (2015).
[47] E. Waks and D. Sridharan, Phys. Rev. A **82**, 043845 (2010).
[48] See Supplemental Material at http://link.aps.org/supplemental/10.1103/PhysRevLett.119.233901 for details.
[49] D. F. Walls and G. J. Milburn, *Quantum Optics* (Springer Science & Business Media, New York, 2007).
[50] P. B. Johnson and R. W. Christy, Phys. Rev. B **6**, 4370 (1972).

[51] M. B. Plenio and P. L. Knight, Rev. Mod. Phys. **70**, 101 (1998).
[52] O. Kyriienko, T. C. H. Liew, and I. A. Shelykh, Phys. Rev. Lett. **112**, 076402 (2014).
[53] Y.-C. Liu, X. Luan, H.-K. Li, Q. Gong, C. W. Wong, and Y.-F. Xiao, Phys. Rev. Lett. **112**, 213602 (2014).
[54] G. P. Acuna, F. M. Mller, P. Holzmeister, S. Beater, B. Lalkens, and P. Tinnefeld, Science **338**, 506 (2012).
[55] M. P. Busson, B. Rolly, B. Stout, N. Bonod, and S. Bidault, Nat. Commun. **3**, 962 (2012).
[56] F. Vollmer, D. Braun, A. Libchaber, M. Khoshsima, I. Teraoka, and S. Arnold, Appl. Phys. Lett. **80**, 4057 (2002).
[57] A. Kuhn, M. Hennrich, and G. Rempe, Phys. Rev. Lett. **89**, 067901 (2002).
[58] A. Kuhn, M. Hennrich, T. Bondo, and G. Rempe, Appl. Phys. B **69**, 373 (1999).
[59] S.-B. Zheng, and G.-C. Guo, Phys. Rev. Lett. **85**, 2392 (2000).
[60] B. Gurlek, V. Sandoghdar, and D. Martin-Cano, arXiv: 1705.04532.